

Evolution of stellar collision products in open clusters. II. A grid of low-mass collisions

Evert Glebbeek and Onno R. Pols

Sterrekundig Instituut Utrecht, Postbus 80000, 3508 TA Utrecht, The Netherlands.

Today

ABSTRACT

In a companion paper we studied the detailed evolution of stellar collision products that occurred in an N -body simulation of the old open cluster M67 and compared our detailed models to simple prescriptions. In this paper we extend this work by studying the evolution of the collision products in open clusters as a function of mass and age of the progenitor stars.

We calculated a grid of head-on collisions covering the section of parameter space relevant for collisions in open clusters. We create detailed models of the merger remnants using an entropy-sorting algorithm and follow their subsequent evolution during the initial contraction phase, through the main sequence and up to the giant branch with our detailed stellar evolution code. We compare the location of our models in a colour-magnitude diagram to the observed blue straggler population of the old open clusters M67 and NGC 188 and find that they cover the observed blue straggler region of both clusters. For M67, collisions need to have taken place recently. Differences between the evolution tracks of the collision products and normal main sequence stars can be understood quantitatively using a simple analytic model. We present an analytic recipe that can be used in an N -body code to transform a precomputed evolution track for a normal star into an evolution track for a collision product.

Key words. Stars: formation, blue stragglers, open clusters and associations: general, M67, NGC 188

1. Introduction

Star clusters are important laboratories for a wide range of astrophysical processes. It has become clear that the evolution of a star cluster is driven by the complex interplay between stellar dynamics and stellar and binary evolution (Portegies Zwart et al. 1999; Hurley et al. 2001). Physical collisions between stars in the dense cluster core play a pivotal role in this interaction. The products of stellar collisions between main-sequence stars potentially stand out as blue stragglers in a colour-magnitude diagram. The blue straggler population of a cluster can therefore be used to study its dynamical history. Since stellar collision products generally have a very different thermal and chemical structure than normal main-sequence stars (Lombardi et al. 1996), detailed calculations of their evolution are required (Sills et al. 1997, 2001).

In a previous paper (Glebbeek et al. 2008) we have developed an efficient procedure to import detailed models of stellar collision products into a fully implicit stellar evolution code and to evolve the remnants well beyond the main sequence. Our work is similar to that of Sills et al. (1997) but our code is faster and much more robust, allowing for the first time a systematic study of stellar merger remnants and an exploration of the parameter space. Glebbeek et al. (2008) studied the evolution of collision remnants that occurred in the N -body simulation of M67 by Hurley et al. (2005) and compared these with the evolution tracks predicted by the prescription of Hurley et al. (2002) as well as tracks of fully mixed versions of the remnants. We found that our merger remnants have shorter main-sequence lifetimes than predicted by either the Hurley et al. (2002) prescription or the fully mixed models. Our models are also brighter than normal stars of the same mass, but not as blue as fully mixed models.

In this work we explore the parameter space for collisions between low-mass main sequence stars relevant for blue straggler formation in old open clusters (such as M67) and place the findings of Glebbeek et al. (2008) in context. A large grid of stellar collisions covering this parameter space was calculated by Freitag & Benz (2005). They mainly focussed on collisions with high impact velocity suitable for the galactic centre and their simulations had insufficient resolution to resolve mixing due to the collision. Our work complements theirs by investigating the mixing as well as the long term evolution of the merger remnants. We describe the detailed structure and evolution of the collision products and discuss their dependence on the collision parameters (masses and time of collision) in §4. We compare the results of our models with observations of blue stragglers in the open clusters M67 and NGC188 in §5. Finally, we show how the global properties of the collision products (luminosity, radius and lifetime) can be described by a simple analytic prescription that can be included in a parametric model of stellar collisions and in N -body simulations (§6). We discuss our results in §7.

2. Initial conditions and parameters of the collisions

The structure of a merger remnant depends on the structure of the two parent stars, the impact parameter of the collision and the relative velocity at infinity. The structure of the parent stars depends on their masses, chemical composition (characterised by their heavy-element content Z) and their evolutionary stage. In this work we have restricted ourselves to a section of this 8-dimensional parameter space.

First of all we assume that the two stars involved in the collision are coeval in the sense that both are at the zero-age main sequence (ZAMS) at $t = 0$ and have the same initial composition, which is a reasonable assumption for stars in clusters.

Placing $t = 0$ at an earlier stage, *e.g.* the onset of deuterium burning rather than the ZAMS, will not greatly affect the outcome of our calculations because appreciable composition gradients only build up on the main sequence and we consider a fairly small mass range. We restrict ourselves to collisions between low-mass main sequence stars (by which here we mean that their combined mass does not exceed $2.4M_{\odot}$, see below) and consider only head-on collisions (*i.e.*, with impact parameter $b = 0$), in essence meaning that we ignore the effect of rotation in the collision product. This is despite the fact that rotation can be of considerable importance for the structure and evolution of the collision product: even for collisions with a small impact parameter the remnant has sufficient angular momentum that a main sequence star of the same mass would need to rotate faster than its breakup rate (Lombardi et al. 1996; Sills et al. 1997). The physical mechanism and timescale on which the collision products lose their angular momentum are unclear. Methods to incorporate the effect of rotation in a one dimensional stellar evolution code treat rotation as a perturbation to a non-rotating stellar model (Endal & Sofia 1976; Pinsonneault et al. 1989; Zahn 1992; Heger et al. 2000). These methods are accurate for rotation rates less than about 60% of the critical (Keplerian) value (Yoon et al. 2004) and it is not clear how to model stars that are even closer to critical rotation. We plan to investigate this problem in future research.

This leaves us with four parameters: the composition, the time of collision t and the masses of the two progenitors. Borrowing nomenclature from the field of binary evolution, we refer to the more massive progenitor as the primary and write its mass as M_1 . Similarly we refer to the less massive progenitor as the secondary and denote its mass by M_2 . With these definitions we can introduce the total initial mass $M = M_1 + M_2$ and the mass ratio $q = M_2/M_1$. To calculate a grid of models we have used the independent parameters Z , t , M and q . We have calculated several grids covering different parts of this parameter space, as listed in Table 1. The grid labelled *M67* covers the parameter space sampled by the *N*-body simulation of Hurley et al. (2005) and is relevant for old open clusters like *M67*. An extension to the *M67* grid is the parameter set labelled *NGC188*, which covers the parameter range of interest for the somewhat older open cluster *NGC188*. Both these grids use an assumed heavy-element content $Z = 0.02$ and an initial hydrogen abundance $X = 0.70$. The total initial masses for the collision products were chosen such that the lower limit is just above the present-day turnoff mass and the upper limit is roughly twice the turnoff mass ($1.18M_{\odot}$ for *NGC188*, $1.29M_{\odot}$ for *M67*); see §5.

We have also computed a grid (labelled *GC*) with $Z = 0.001$ and $X = 0.757$ that is suitable for comparison with globular clusters. In the presentation of our results we will mostly focus on the *M67* and *NGC188* grids but unless otherwise indicated our results apply to the $Z = 0.001$ grid as well.

3. Tools

The method we use in our study has been described in detail in a separate paper (Glebbeek et al. 2008) (hereafter Paper I), so we refer the interested reader to that paper for more details about the procedure of calculating the models and provide just a brief summary here.

For each collision we evolve models of the progenitor stars to the time of collision and then merge the two stars. The structure of the merger remnants is calculated using the Make Me A Star

(MMAS) code developed by Lombardi et al. (2002). This code uses the realisation that in low mass stars the quantity

$$A = \frac{P}{\rho^{5/3}} \quad (1)$$

increases outward. The quantity A is closely related to the entropy and the tendency of A to increase reflects the tendency of low entropy material to sink to the centre of the collision product. For this reason the procedure by which the remnant profile is constructed is known as *entropy sorting*.

Our evolution code is a version of the STARS code developed by Eggleton (1971) and updated by others (Pols et al. 1995). Nuclear reaction rates are from Caughlan & Fowler (1988) and Caughlan et al. (1985) and we use opacities from Rogers & Iglesias (1992) and Alexander & Ferguson (1994). The assumed heavy-element composition is scaled to solar abundances (Anders & Grevesse 1989). Chemical mixing due to convection (Böhm-Vitense 1958; Eggleton 1972) and thermohaline mixing (Kippenhahn et al. 1980) is taken into account. All models are computed with a mixing-length ratio $l/H_p = 2.0$. As in Paper I, we have neglected convective overshooting in all models in this work.

4. Properties and structure of collision products

In this section we present the structure and evolution of the merger remnants. We will discuss how the structure of the parent stars affects the structure of the remnant. Details for all our collision models are listed in Table 4 for $Z = 0.02$ models and in Table 3 for $Z = 0.001$ models. Both these tables are available in the Online version of this paper.

4.1. Mass loss from the collision

A fraction ϕ of the total mass $M_1 + M_2$ of the progenitor stars is lost during the collision. The fraction ϕ is, for central collisions, estimated in MMAS as

$$\phi = C \frac{q}{(1+q)^2} \frac{R_{1,0.86} + R_{2,0.86}}{R_{1,0.5} + R_{2,0.5}}, \quad (2)$$

(Lombardi et al. 2002), where $R_{n,0.86}$ and $R_{n,0.5}$ are the radii containing 86% and 50% of the mass of parent star n (1 or 2). The constant $C = 0.157$ is determined by calibration to SPH calculations. Typical values of ϕ are in the order of a few percent. A reasonable approximation over the range of our grid is (see Table 4)

$$\phi = 0.3 \frac{q}{(1+q)^2}. \quad (3)$$

Material lost from the stars in the ejecta originates from the envelopes of the parent stars and has the composition of the parent star envelope.

4.2. Structure of the progenitor stars

We can distinguish four different collision scenarios between main sequence stars based on the structure of the progenitor stars and the collision product. Low mass main sequence stars ($\leq 1.2M_{\odot}$) have radiative cores while main sequence stars of higher mass have a convective core. This leads to four possible scenarios for a collision:

1. Convective + Convective \rightarrow Convective

Table 1. Values used for the different grid parameters. The grid spacing is listed between parentheses. Note that the grids labelled *M67* and *NGC188* overlap in part of their age range. We have calculated models for two extra mass ratios for a limited mass range in the *M67* grid to more clearly resolve trends at high and low mass ratios.

Name	Z	t [Myr]	$M[M_{\odot}]$	q
M67	0.02	2800, 3100, 3400, 3700	1.5–2.4 (0.1)	0.4–1.0 (0.2)
			1.5–2.0 (0.1)	0.5, 0.9
NGC188	0.02	3400, 3700, 4200, 4700, 5200, 5700	1.2, 1.3, 1.4, 1.6, 1.8, 2.0, 2.2	0.4–1.0 (0.2)
GC	0.001	8000–12500 (1500)	0.8–1.3 (0.1)	0.4–1.0 (0.2)

2. Convective + Radiative → Convective
3. Radiative + Radiative → Convective
4. Radiative + Radiative → Radiative

The composition profile of a collision remnant is determined by the entropy profiles of the progenitor stars, which is in turn determined by their masses and their age. If a star has a convective core the material from the core will have a constant entropy, which directly affects the composition profile in the remnant and its subsequent evolution. In a star with a radiative core the entropy increases outward.

The first case will generate remnants with masses $> 2.4M_{\odot}$ and will be the topic of a future paper. The second case occurs in our grid for the higher mass collision products ($M > 1.7M_{\odot}$) at extreme mass ratios ($q > 0.5$) and is relevant for clusters where the turnoff mass is larger than $1.2M_{\odot}$. The third case makes up the majority of the collision products in our grid and is relevant for old open clusters as well as globular clusters. The main difference with case 2 is that in case 2 the core of the primary has an almost flat entropy profile whereas in case 3 the entropy profile is smoother. The final case is only relevant for clusters where the turnoff mass is below $1.2M_{\odot}$. In younger clusters the collision products of these collisions would be hidden among normal main sequence stars and not stand out as blue stragglers. The progenitor stars are essentially unevolved at the time of collision and the outcome of such a merger is a new unevolved main sequence star.

4.3. Composition profile

During a collision material from one parent star is mixed with material of the same entropy from the other star (since it ends up in the same location in the collision product). However, if one of the two stars has a convective core the material from the core can retain its identity because of the nearly flat entropy profile. This can lead to a very steep composition gradient in the remnant.

On the ZAMS lower mass stars have a lower central entropy than higher mass stars (their cores are denser), which means that in a collision between unevolved stars material from the lower mass star will sink to the centre of the collision product. As a result of stellar evolution, the entropy in the core will decrease (the core becomes more compact). Since more massive stars evolve more quickly, the central entropy will decrease more rapidly in massive stars than it will in low mass stars.

Figure 1 shows a number of evolution tracks in the $\log \rho_c - \log T_c$ plane. The location of the ZAMS is indicated by a thick solid line on the left and the location of the terminal age main sequence (TAMS) by a thick solid line on the right. Evolution tracks are dotted and labelled with the mass of the star and two isochrones are shown, one for 1000 Myr and one for 3100 Myr. Two lines of constant entropy across different stellar models are also drawn for different ages. The shaded region indicates the location where the entropy is lower than in the core of a $0.75M_{\odot}$

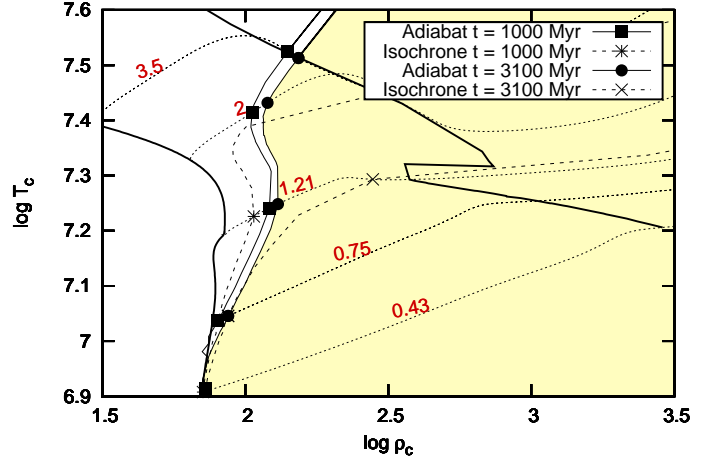


Fig. 1. Evolution tracks of low mass stars in the $\log \rho_c - \log T_c$ plane. Bold lines indicate the locations of the ZAMS (left) and TAMS (right). Dotted lines are evolution tracks, labelled with the ZAMS mass. The solid lines marked with ■, ● are lines of constant entropy across different stellar models, the dashed lines marked with *, × are isochrones. The shaded region indicates the region where the central entropy is lower than that of a $0.75M_{\odot}$ star at 3100 Myr.

star at $t = 3100$ Myr. The $t = 3100$ Myr isochrone lies almost completely within this region, indicating that in a collision with a more massive star at this age the core of the primary sinks to the centre of the collision product. Conversely, part of the $t = 1000$ Myr isochrone lies to the left of the line of constant entropy at that age, indicating that in a collision with a more massive star, up to $\approx 1.9M_{\odot}$, the secondary star will sink to the centre.

For the composition profile in the collision product we can roughly distinguish three cases, which we will denote by ‘M’, ‘S’ and ‘P’ for ‘mixed core’, ‘secondary core’ and ‘primary core’ respectively. These are illustrated in Figure 2. The part of the parameter space in the grid for which each of these cases occurs is illustrated in Figure 3 and listed in Table 4.

4.3.1. Case M

If the mass difference between the two colliding stars is small (the mass ratio is close to 1), the colliding stars have very similar entropy and composition profiles. The composition profile of the collision product will resemble a stretched version of the composition profile in the progenitor stars. This situation is illustrated by the top left panel in Figure 2. There can be a small molecular weight inversion near the centre if most of the material in the core comes from the secondary star. This case is indicated by □ in Figure 3. In Figure 1 this means that the two models are on or close to the line of constant entropy.

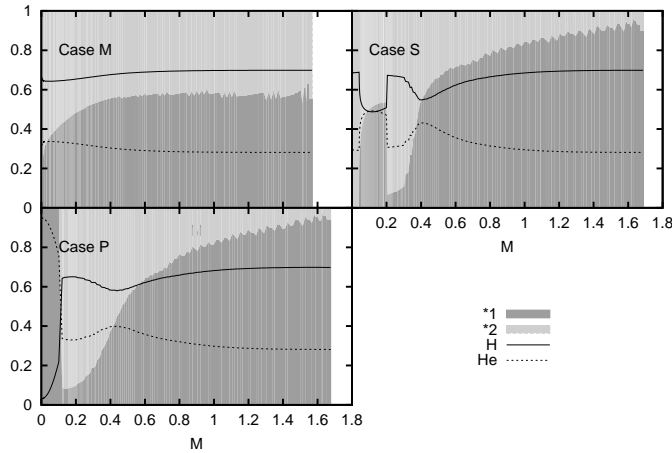


Fig. 2. Diagram showing the distribution of material from the parent stars within three of the collision products: $t = 2800$, $q = 0.8$, $M = 1.7$ (corresponding to case *M*, see text) and $t = 2800$, $q = 0.4$, $M = 1.8$ (case *S*) and $t = 3700$, $q = 0.4$, $M = 1.8$ (case *P*) for the bottom row. The dark shading indicates the fraction of material from the primary while the lighter region shows the fraction of material from the secondary. Overplotted are the abundances by mass fraction of hydrogen (solid) and helium (dotted).

4.3.2. Case P

If the primary is sufficiently evolved that its core entropy is lower than that of the secondary, the core of the primary ends up in the centre of the collision product. In Figure 1 this means that the primary is in the shaded region of the diagram. In this case the core of the merger remnant has a reduced hydrogen content with a very steep increase in hydrogen abundance at its edge and possibly a molecular weight inversion further out as well. A hydrogen burning shell can form at the edge of the core (see §4.4). This is the situation in the lower left panel of Figure 2 and is marked in Figure 3 with Δ . An extreme example of this case occurs when the primary is at the end of the main sequence. The hydrogen depleted core of the primary sinks to the centre of the collision product, producing a new star with a hydrogen depleted core. In other words, collisions involving turnoff stars produce turnoff stars, in agreement with Sills et al. (1997).

4.3.3. Case S

If the entropy in the core of the primary is larger than the entropy in the core of the secondary the secondary will sink to the centre of the collision product. In terms of Figure 1 the primary is to the left of the shaded region. The core of the collision product will be hydrogen-rich, with a helium rich layer on top of it, leading to a pronounced molecular weight inversion. This is the upper left situation in Figure 2 (a $*$ in Figure 3). This case will appear for collisions between main sequence stars when the mass ratio of the colliding stars is small (~ 0.4). If the mass ratio is even smaller ($\lesssim 0.2$), this will happen even after the primary has already evolved off the main sequence.

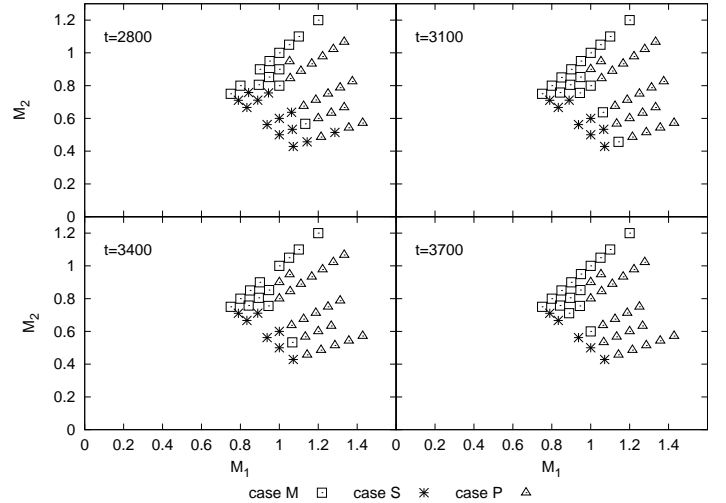


Fig. 3. Illustration of the different cases for the composition profiles in the collision products and the grid parameters for which they occur.

4.4. Reignition of hydrogen and mixing

Initially there is little or no nuclear burning in the core of the collision products and nuclear burning is unimportant as an energy source during the contraction to the main sequence.

Because the core of the collision product has the entropy of a lower mass star it lies on a lower adiabat than the core of a main sequence star of the same mass and composition. In practice, this means that the collision product is initially to the right of its main sequence position in the $\rho_c - T_c$ plane, at higher central densities. In order for the star to come into thermal equilibrium the entropy in the core needs to increase. The core will first expand and then heat up (see Paper I). Once hydrogen burning takes over as the main energy source the evolution of the collision product proceeds analogously to that of a normal main sequence star but with an abnormal composition profile (again see Paper I).

If there is a steep composition gradient at the edge of the core (when one of the two stars had a convective core), it is possible for the nuclear energy generation rate to peak at this location due to the composition dependence of the reaction rate. In effect, hydrogen will burn in the core as well as in a shell outside the core. This hydrogen burning shell is a transient feature that is destroyed when mixing reduces the steepness of the composition gradient. The hydrogen burning shell is important because it can drive a convection zone that mixes the layers above it. Examples of the mixing regions during the contraction phase in each of the three cases in Figure 2 are shown in Figure 4.

Because the material outside the core can be hydrogen-rich, convection can bring extra hydrogen to the core, effectively rejuvenating the star. How much hydrogen is mixed into the core depends on mixing processes in the layer outside the core.

Helium-rich material on top of a layer of hydrogen-rich material causes a molecular weight inversion, which gives rise to thermohaline mixing (Kippenhahn et al. 1980). The material with higher molecular weight is supported by thermal buoyancy. Diffusion of heat from the material causes it to lose buoyancy and sink due to its higher mean molecular weight. The mixing continues until the molecular weight inversion is removed. Thermohaline mixing is important in the collision products during the contraction phase in the cases where material from the

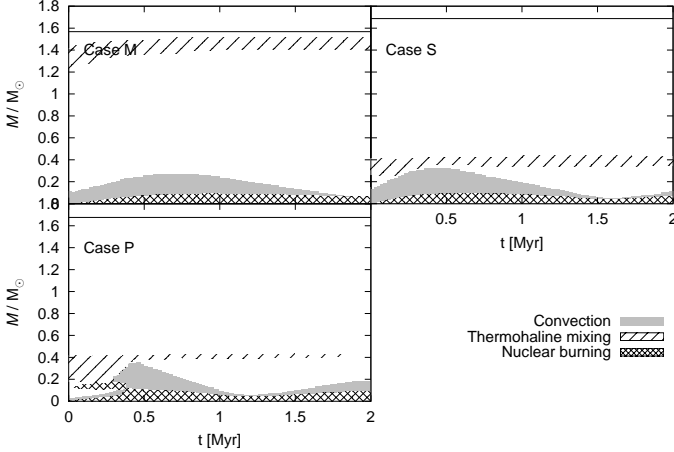


Fig. 4. Kippenhahn diagrams showing the mixing regions during the contraction phase for the same collision products as shown in Figure 2.

core of the primary overlies material from the secondary, which happens for cases *P* and *S*, discussed in §4.3 and shown in Figure 4. By the time the collision products reach the main sequence the molecular weight inversion has been smoothed out. As a result more helium has been mixed into the centre of the collision product than would have been the case if thermohaline mixing had been ignored. This reduces the amount of hydrogen available for nuclear burning and decreases the lifetime of the collision product.

A hydrogen burning shell at the edge of the core can drive a convection zone that mixes in material from the layers above. This material can be either hydrogen-rich or helium rich, depending on the particular case. The convection zone can connect to the thermohaline layer, which means extra helium is mixed into the inner region of the star.

When the convective core is formed it can in turn connect to the convection zone driven by the burning shell (Figure 4, lower left panel). If there is no burning shell, it can connect to the thermohaline layer (Figure 4 upper left panel). In either case the end result is that the interior of the collision product is mixed below the molecular weight inversion. This produces a large central region that has been enhanced in helium and is larger than the convective core itself. The net effect is comparable to that of a star in which the convective core was larger initially but has shrunk.

Outside the mixed region, the composition profile is shallower than in a normal star of the same mass. This affects the structure of the star most strongly during the main sequence although it continues to affect the star during later evolutionary stages.

4.5. Main sequence evolution

Once the merger remnant has attained thermal equilibrium its further evolution proceeds similarly to that of a normal star of the same mass. In particular, the shape of the evolution track in a Hertzsprung-Russell diagram is the same. The composition profile modifies the evolution mainly in two ways: by affecting the lifetime and by affecting the luminosity. A typical evolution track is shown in Figure 5.

The luminosity is affected by the higher helium content of the envelope. This affects the structure of the star through the equation of state (due to the mean molecular weight) and the

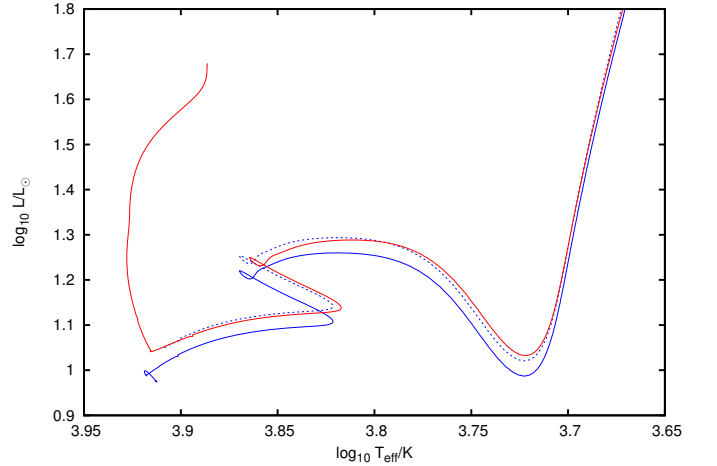


Fig. 5. Evolution track of the $t = 2800$, $q = 0.8$, $M = 1.9$ remnant with a mass of $1.75M_{\odot}$ (top solid line) compared with the evolution track of a normal star of the same mass (bottom solid line). The shape of the evolution tracks after the contraction of the merger remnant is very similar, but the merger track is offset to higher luminosity and is slightly cooler at the end of the main sequence. The dashed line is a shifted version of the main sequence track according to equations (13) and (19), see §6.

opacity, as discussed in Paper I, and results in a larger radius and higher luminosity. Because the surface layers do not show helium enhancement the effective temperature is not strongly affected, although there is a systematic trend that the coolest part of the track (just before hydrogen exhaustion at the end of the main sequence) is shifted to slightly lower temperatures. Shifts in the luminosity and effective temperature are listed in Table 4 for all our merger remnants.

The remaining lifetime of the star is reduced by the higher luminosity, but also by the central hydrogen abundance which is lower than the abundance in the envelope. Because of this the merger remnants do not resemble zero-age main sequence (ZAMS) stars after they settle down and are both redder and brighter than ZAMS stars of the same mass.

While on the Hertzsprung gap tracks of the merger remnants are still brighter than tracks of normal stars of the same mass. On the giant branch the difference between the two tracks vanishes. When the first dredge-up occurs the convective envelope enters the layer where the composition had been modified by the merger. This enhances the post-dredge-up abundances of helium and nitrogen and reduces the abundance of carbon compared to a normal red giant (see Paper I for more details).

4.6. The effect of lower metallicity

The heavy-element abundance Z affects the structure and evolution of stars. In general stars with a lower Z are hotter, more luminous and more compact than stars of the same mass at higher Z . The mass at which a convective core develops is higher and the lifetime is reduced.

This changes the structure of merger remnants in subtle ways. For instance, the relative rate at which the progenitor stars evolve along the main sequence is different for $Z = 0.02$ and $Z = 0.001$. This means that if we consider a $Z = 0.001$ collision at a time when the primary has passed the same fraction of its main sequence lifetime, the secondary will not have spent the same fraction of its main sequence lifetime as in the $Z = 0.02$

Table 2. Ages determined from isochrone fitting for adopted values of distance modulus and reddening. See Pols et al. (1998) for details.

Name	\log_{10} age/yr	M_{to}	[Fe/H]	$m - M$	$E(B - V)$
M67	9.60	1.29	-0.06	9.60	0.032
NGC 188	9.76	1.18	-0.06	11.40	0.12

collision. Qualitatively the description given in the previous subsections remains valid for smaller Z . The data for the merger remnants calculated for our grid are listed in Table 3.

The mass loss from the collisions is slightly lower than for the $Z = 0.02$ grid although $C = 0.3$ is still a reasonable guess. The reason for this can be seen from (2): the stars at lower Z are more centrally condensed than at higher Z and the ratio $(R_{1,0.86} + R_{2,0.86})/(R_{1,0.5} + R_{2,0.5})$ is smaller.

5. HRD distributions: comparison with M67 and NGC188

In this section we compare the predicted locations of the collision products from our grid with the observed blue stragglers in the open clusters M67 and NGC188. For both of these clusters Pols et al. (1998) determined isochrone fits. For consistency we employ the same cluster parameters they used, as listed in Table 2.

In order to make the comparison between our models and the observations it is necessary to convert the theoretical surface parameters ($L, T_{\text{eff}}, \log g$) to the observable magnitude and colour ($M_V, B - V$). This conversion is done using the atmosphere models from Kurucz (1992) with empirical corrections from Lejeune et al. (1997).

Figure 6 shows the observed colour-magnitude diagram of M67 (\bullet). The V and $B - V$ data is taken from Sandquist (2004) supplemented with Montgomery et al. (1993) for blue stragglers that were missing from the Sandquist (2004) data. Membership information (based on proper motions) is taken from Sanders (1977). Sandquist (2004) gives a distance modulus $m - M = 9.60$ and reddening $E(B - V) = 0.03$, consistent with the values used by Pols et al. (1998) to construct the 4 Gyr isochrone. The location of the collision remnants at 4 Gyr are plotted with different symbols, corresponding to the different times of collision. It is important to stress that our model is not a population synthesis model, so one should not draw conclusions from the density of the model points.

Our models lie in the observed blue straggler region. Some of the lower-mass merger remnants with masses below the turnoff appear among the normal main-sequence stars. The bluest blue straggler (S977 with $M_V = 0.413$ and $B - V = -0.126$, Mathys 1991) is clearly outside the region covered by our models, but it is thought to have a mass larger than twice the turnoff mass (Sandquist 2005) and therefore cannot be formed by a single collision event. A few other blue stragglers are somewhat bluer than the region covered by our models. They are apparently single stars and are thus very likely to be the result of a stellar merger. Their blue positions can be explained if they have undergone much stronger internal mixing than our models, or if they have been formed more recently and are in that sense younger than our models. These blue stragglers are all slow rotators ($v \sin i \leq 120$ km/s) compared to normal stars of the same spectral type (Mathys 1991), suggesting that rotational mixing has not played a major role in their evolution. We therefore prefer the second explanation, which suggests that M67 is dynam-

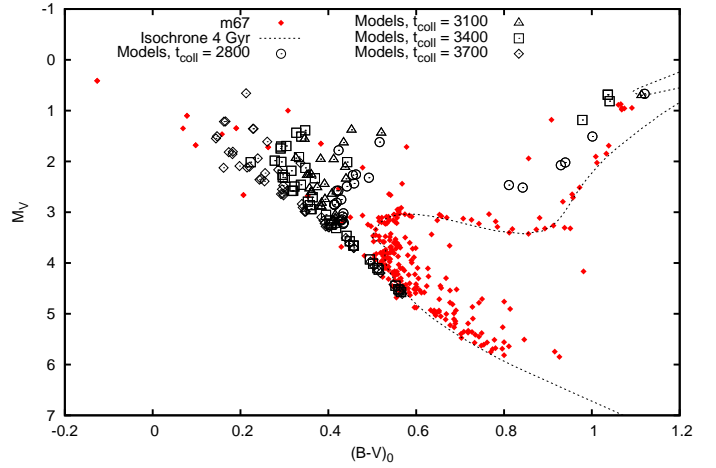


Fig. 6. Observed colour-magnitude diagram of the open cluster M67, with blue stragglers highlighted and the positions of the stars in our collision grid at the age of M67 overplotted. Different symbols correspond to different times of collision, as indicated.

cally active, in other words, collisional blue stragglers are still being formed. This conclusion is consistent with the N -body model of Hurley et al. (2005).

A number of our merger remnants have evolved beyond the end of the main sequence and appear on the giant branch but to the blue of the normal cluster giant branch, indicating that merger remnants can still stand out in the CMD even after the main sequence has ended. Two stars in M67 are located in this region (S1040 and S1273); both are spectroscopic binaries as well as unusual X-ray sources (van den Berg et al. 1999). It is not clear whether these stars are merger remnants, their unusual location may also be the result of a superposition of a giant and a turnoff star. In the case of S1040 the companion is probably a white dwarf and the orbit is circular (Mathieu et al. 1990), so the system has likely undergone mass transfer.

Figure 7 shows the comparison with NGC188, with $V, B - V$ and membership probabilities taken from Platais et al. (2003). Although NGC188 is known to be older than M67, different authors give different age estimates (von Hippel & Sarajedini 1998; Platais et al. 2003; Carraro et al. 1994). We adopt $m - M = 11.4$ and $E(B - V) = 0.12$ and an age of 5.8 Gyr, as in Pols et al. (1998). By contrast, Bonatto et al. (2005) find $m - M = 11.1$ and $E(B - V) = 0.0$ from fitting a $t = 7$ Gyr Padova isochrone.

Our models fill a larger region than the observed blue straggler region, indicating that NGC188 has not formed massive blue stragglers recently. This suggests that it is less dynamically active than M67. As for M67 we note that a number of merger remnants are beyond the main sequence and on the giant branch, again parallel to the cluster giant branch.

6. Analytical description of results

To quantify the results of our collision calculations and compare the evolution tracks of the collision products with evolution tracks of normal single stars it is necessary to specify which models should be compared. In particular, we need to define an equivalent main sequence star model.

Apart from the mass M of the collision product the remaining lifetime is a good parameter to consider. For this reason it is

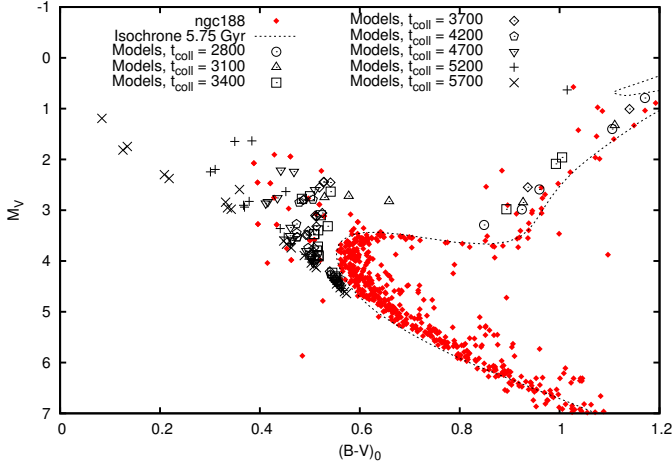


Fig. 7. As Figure 6 for NGC 188

convenient to introduce the fractional age f , which is the age of a star expressed in units of its main sequence lifetime,

$$f = \frac{t}{\tau_{\text{MS}}} \quad (4)$$

where t is the absolute age and $\tau_{\text{MS}} = \tau_{\text{MS}}(M, Z)$ is the main sequence lifetime of a star of mass M and composition specified by Z . As long as the star is on the main sequence, $0 < f < 1$. We define the apparent age f_{app} of the collision product as the fractional age of a normal main sequence star with the same remaining lifetime t_{MS} . These two quantities are related by

$$t_{\text{MS}} = \tau_{\text{MS}}(1 - f_{\text{app}}). \quad (5)$$

In practice, we know t_{MS} from the detailed models (see Table 4) for the collision products and we can thus determine f_{app} . If we can predict f_{app} from the global properties of the parent stars we can predict the collision product lifetime. In the following we will describe a formalism that allows us to do this using only standard stellar models and we give a set of transformation rules that can be used to transform a standard stellar evolution track to approximate the track of a merger remnant. By a standard evolution track we mean the evolution track of a single star that is evolved from the zero-age main sequence. For the standard tracks one can use the Hurley et al. (2000) recipe, or interpolate on a grid of single star models. Our recipe can be used to improve the accuracy of evolution tracks for merger remnants in star cluster simulations.

6.1. Collision product lifetimes

In normal main sequence stars there is a unique relation between the amount of hydrogen and the age of the star. Collision products show a similar relation. Although it might seem better to relate the age of the star to the amount of hydrogen in the core rather than the total amount of hydrogen, in practice this is not a good measure of the age of the star for collision products because mixing as described in §4.4 can increase the central hydrogen abundance compared to its post-collision value.

The relation between the amount of hydrogen and the age of the star is the starting point for a relation between the global properties of the parent stars and the apparent age f_{app} of the collisions product. Let's consider a simple stellar model that divides the star in two parts: a core where hydrogen is burned to

Table 3. Coefficients for the fitting formula (8) for q_c . The first column lists values that are valid in the mass range $0.4 - 75 M_{\odot}$ for $Z = 0.02$, the second column lists coefficients that give a more accurate fit in the mass range $0.4 - 4.0 M_{\odot}$. The third and fourth columns are similar but for $Z = 0.001$. The bottom row (rms) gives the root mean square error of the fits.

c	$Z = 0.02$		$Z = 0.001$	
	$0.4 - 75 M_{\odot}$	$0.4 - 4 M_{\odot}$	$0.4 - 75 M_{\odot}$	$0.4 - 5 M_{\odot}$
c_1	-0.685213	-0.999710	-0.682671	-0.873596
c_2	0.289269	0.276843	0.185036	0.165455
c_3	0.0123223	0.0393513	0.00658021	0.0158297
c_4	$3.3357e-6$	0	$7.5450e-7$	0
c_5	2.70964	2.75579	2.71437	2.72675
c_6	1.44963	-1.70434	0.334367	-1.33733
c_7	0.629121	1.46625	0.343889	0.644498
c_8	0.000493117	0	0.000185160	0
rms	1.4%	1.2%	1.7%	1.3%

helium and an envelope which is not affected by nuclear burning on the main sequence. The core has a mass fraction q_c of the total mass M . Such a model is not really applicable to low-mass stars, which do not have a well-defined core. However, we can generalise the model by defining q_c to be the fraction of hydrogen that is burned during the main sequence, so that

$$q_c = \frac{X_0 - \langle X \rangle_{\text{TAMS}}}{X_0}, \quad (6)$$

with X_0 the initial (ZAMS) hydrogen fraction. We can think of q_c as being the *effective core* mass fraction. If we approximate the nuclear burning rate as steady, the average (total) amount of hydrogen follows from the relative age f as

$$\langle X \rangle(t) = X_0(1 - q_c f). \quad (7)$$

In practice, q_c will depend on the stellar mass M and composition Z and needs to be found from detailed stellar models. It is convenient to have an analytic approximation for $q_c(M)$. We use the rational function

$$q_c(M) = \frac{1 + c_1 M + c_2 M^3 + c_3 M^5 + c_4 M^7}{c_5 + c_6 M^2 + c_7 M^4 + c_8 M^6} \quad (M \text{ in } M_{\odot}). \quad (8)$$

The coefficients c_i have been found by least-squares fitting to detailed models calculated with the STARS code for masses in the range $M = 0.4 \dots 75 M_{\odot}$. These models were computed without convective overshooting. The fitting coefficients are listed in Table 3. In the mass range $0.4 \dots 4.0 M_{\odot}$ a somewhat more accurate fit is possible without the terms involving M^6 and M^7 (second and fourth column in Table 3); the quality of this fit for $Z = 0.02$ can be checked against Figure 8. It is of course also possible to interpolate on a table of detailed models.

To find an expression for f_{app} we first need to know the amount of hydrogen in the collision product. To do this correctly we should consider the material that is ejected during the collision. This comes from the progenitor star envelopes and therefore has the initial ZAMS hydrogen abundance X_0 . If ϕ is the fraction of mass lost during the collision (see §4.1) then the mass M of the collision product is $M = (1 - \phi)(M_1 + M_2)$. The average hydrogen abundance $\langle X \rangle$ in the collision product immediately after the collision is then given by

$$M \langle X \rangle = M_1 \langle X \rangle_1(t) + M_2 \langle X \rangle_2(t) - \phi(M_1 + M_2)X_0. \quad (9)$$

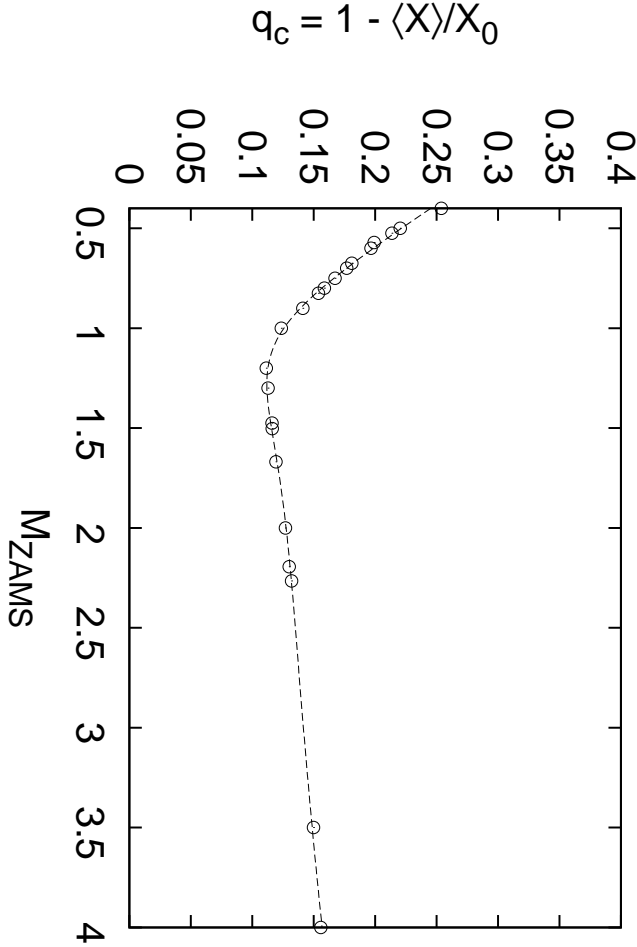


Fig. 8. Effective core mass fraction for main sequence stars against ZAMS mass, for $Z = 0.02$ (\odot). The fitting formula (8) in the mass range $0.4 - 4.0 M_{\odot}$ is shown as a dashed line.

Inserting (7) for the hydrogen abundance in the parent stars and solving for $\langle X \rangle$,

$$\langle X \rangle = X_0 \left(1 - \frac{1}{1 - \phi} \frac{q_{c,1} f_1 + q_{c,2} f_2 q}{1 + q} \right). \quad (10)$$

The equivalent age f_{app} is determined by the amount of hydrogen q_M that gets mixed into the burning region through

$$\langle X \rangle = X_0 (1 - q_M f_{\text{app}}). \quad (11)$$

As already mentioned in §4.4 the larger fraction of processed material within the merger remnant has an effect that is comparable to that of a star with an initially larger core mass. Setting $q_M = \alpha q_c(M)$, we find f_{app} from (10) as

$$f_{\text{app}} = \frac{1}{\alpha q_c(M)} \frac{1}{1 - \phi} \frac{q_{c,1} f_1 + q_{c,2} f_2 q}{1 + q}. \quad (12)$$

The parameter α parametrises the amount of mixing during the collision and settling to the main sequence, with $\alpha = 1$ meaning no mixing at all and $\alpha = 1/q_c(M)$ meaning homogeneous mixing. Our expression (12) is a generalisation of equation (69) in Tout et al. (1997) and (80) in Hurley et al. (2002), which are recovered in the special case $\phi = 0$, $q_{c,1} = q_{c,2} = q_c(M) = 1/10$ and $\alpha = 1/q_c(M)$.

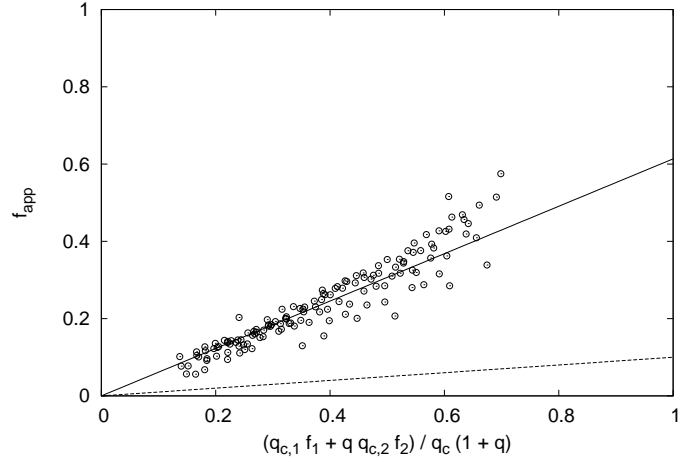


Fig. 9. The predicted apparent age according to (12), for $\alpha = 1.67$ (solid line). The detailed models are indicated by \odot . The dashed line is the prescription from Hurley et al. (2000).

The parameter α can be determined from the models in our grid because all other factors in equation (12) are known. In principle it should depend on the evolutionary stages of the two stars involved in the collision, but in practice the value $\alpha = 1.67$ works well for all models in our $Z = 0.02$ grid, while $\alpha = 1.43$ works well for our $Z = 0.001$ grid.

Figure 9 compares the predicted lifetime according to (12) to the lifetime from our detailed models. Overall agreement is very good, although the detailed models show more scatter. The dashed line is the prescription from Hurley et al. (2000), which predicts much longer lifetimes, especially for collisions involving very evolved stars. This increases the predicted number of observable blue stragglers formed through collisions by up to a factor 2 compared to our detailed models.

6.2. Collision product luminosities

The luminosity of the collision products follows very well from the homology relation (Kippenhahn & Weigert 1990)

$$L_{\text{merger}} = L_{\text{MS}} \left(\frac{\mu_{\text{merger}}}{\mu_{\text{MS}}} \right)^4. \quad (13)$$

Here, μ_{merger} is the average mean molecular weight in the collision product at the start of the main sequence, which is the same as the average mean molecular weight after the collision because the contraction phase is fast enough that composition changes due to nuclear reactions can be ignored. The average mean molecular weight of the main sequence model μ_{MS} needs to be chosen at the equivalent stage of evolution. Because the shift in effective temperature is small we can choose the point in the evolution track with the same T_{eff} as the equivalent point. The averages of the mean molecular weight need to be calculated with respect to the mass (as opposed to the radius), which is the same as averaging over all particles.

It is possible to get an estimate for the mean molecular weight using the simple model (7). For a fully ionised hydrogen/helium mixture, the mean molecular weight can be approximated by (e.g. Weiss et al. (2004))

$$\mu^{-1} = 2X + \frac{3}{4}Y + \frac{1}{2}Z, \quad (14)$$

or, by eliminating the helium abundance Y ,

$$\mu^{-1} = \frac{1}{4} (5X + 3 - Z). \quad (15)$$

Then

$$\frac{\mu_{\text{merger}}}{\mu_{\text{MS}}} = \frac{5 \langle X \rangle_{\text{MS}} + 3 - Z}{5 \langle X \rangle_{\text{merger}} + 3 - Z}. \quad (16)$$

For the main sequence star we can use (7) directly but to match the hydrogen abundance of the merger remnant we use a modified version of (7),

$$\langle X \rangle_{\text{merger}} = X_0 (1 - \beta - \alpha q_c f_{\text{app}}). \quad (17)$$

Physically, this extra parameter is necessary because f_{app} was calibrated to the main sequence timescale τ_{MS} for a normal star. The collision products behave more like stars with a different initial composition and can have a different main sequence timescale. In other words, f_{app} does not represent the evolutionary stage of the collision product, just its remaining lifetime. Mathematically, the need for an extra parameter arises because we are now fitting two quantities (the lifetime and the hydrogen abundance).

The offset should vanish if the progenitor stars were ZAMS stars (in which case $f_{\text{app}} = 0$) or if there was no mixing during the collision ($\alpha = 1$). This is satisfied if $\beta \propto (\alpha - 1)f_{\text{app}}$. We find that setting $\beta = (\alpha - 1)q_c f_{\text{app}} / (1 - q_c)$ gives a good match for all collisions in our grid. Inserting this expression in (17) gives

$$\langle X \rangle_{\text{merger}} = X_0 \left(1 - \alpha q_c \frac{\alpha(2 - q_c) - 1}{\alpha(1 - q_c)} f_{\text{app}} \right). \quad (18)$$

Setting $\delta \langle X \rangle = \langle X \rangle_{\text{merger}} - \langle X \rangle_{\text{MS}}$ and introducing $\mu_0 = 5 \langle X \rangle_{\text{MS}} + 3 - Z$,

$$\frac{\mu_{\text{merger}}}{\mu_{\text{MS}}} = \frac{\mu_0}{\mu_0 + 5\delta \langle X \rangle} \approx 1 - 5 \frac{\delta \langle X \rangle}{\mu_0}. \quad (19)$$

From (7) and (11),

$$\delta \langle X \rangle = X_0 q_c f_{\text{app}} \frac{(2 - q_c)(1 - \alpha)}{1 - q_c}. \quad (20)$$

Physically, $\alpha > 1$ and we see that in that case $\langle \mu \rangle_{\text{merger}} > \langle \mu \rangle_{\text{MS}}$, as we would expect.

The luminosity shift predicted by our analytic prescription is shown in Figure 5 (dashed line). The main sequence part of the track is very well represented by our prescription, although the hook at the end is slightly too hot. Even the Hertzsprung gap and the giant branch are very well matched with the same shift.

6.3. Collision product effective temperatures and radii

The effective temperature of the merger remnants is not very different from that in a normal star of the same mass (see the listed temperature shifts in Table 4), but the reddest point of the main sequence hook is slightly cooler.

Since the effective temperature of the collision products is very similar to that of normal stars it is possible to use the effective temperature expected for normal stars. Taking the luminosity from (13) the radius of the collision product follows from the Stefan-Boltzmann law, so that

$$R_{\text{merger}} = R_{\text{MS}} \left(\frac{\mu_{\text{merger}}}{\mu_{\text{MS}}} \right)^2. \quad (21)$$

7. Discussion and conclusions

We have calculated a grid of stellar evolution models for the remnants of collisions between main sequence stars. These models improve on the models in the literature by using a better model for the initial structure of the merger remnant (Bailyn & Pinsonneault 1995) or by studying a larger portion of the t, q, M parameter space (Sills et al. 1997).

We have compared the position of our models in the Hertzsprung-Russell diagram with the observed blue straggler regions in the open clusters M67 and NGC 188 and found that our models can populate the blue straggler region, provided that the blue stragglers in M67 are relatively ‘young’ and those in NGC 188 are relatively ‘old’.

We have used our results to formulate a recipe that can be used to transform a normal evolution track, which can be obtained from fitting formulae (Hurley et al. 2000) or by interpolation on a table (e.g. Pols et al. 1998; Girardi et al. 2002). This can be used to improve the treatment of collisions in N -body calculations and population modelling.

Our models do not include the effect of rotation. Rotation can modify our results in two ways: collision products need to lose angular momentum and therefore mass to reach hydrostatic equilibrium and rapid rotation can induce mixing. It is clear that for a collision product to survive angular momentum must be lost but the mechanism by which this occurs is unclear. Magnetic fields may be involved, but their role is not well understood. Rotational mixing can enrich the stellar envelope in helium, increasing the luminosity and extending the stellar lifetime. By ignoring rotation we have assumed that an efficient mechanism to remove the angular momentum operates that spins the star down sufficiently that rotational mixing is not important for the long-term evolution. The fact that blue stragglers in M67 are observed to be rotating slowly (Mathys 1991) can be interpreted as an indication that such an efficient mechanism for removing angular momentum does operate in reality.

Although our models can fill the observed blue straggler region in M67 and NGC 188, this does not directly give information about the expected distribution of blue stragglers in the colour magnitude diagram because the models need to be weighted with the probability for each collision. This requires a dynamical (or statistical, e.g. Monte-Carlo) model for the cluster evolution.

There are several directions for future research that could be explored. From the side of cluster modelling it is interesting to study the effect of our predicted corrections to the evolution tracks on the number of expected blue stragglers and on the blue straggler luminosity function. On the topic of detailed modelling of merger remnant evolution, including rotation and rotational mixing (extending the work of Sills et al. 2001, 2005) is a logical next step. However, this needs to be coupled with a mechanism for angular momentum loss from the merger remnant, which requires a better understanding of mass loss from rapidly rotating low mass stars, possibly involving magnetic fields as well. A simple equilibrium dynamo may not be adequate to model the magnetic field of a merger remnant, which might be very different from the magnetic field of a normal star following the collision. Magnetohydrodynamic models of stellar mergers and stellar evolution models including magnetic fields are also relevant in this light and are a logical next step.

Acknowledgements. We thank the referee, Alison Sills, for valuable comments and Frank Verbunt for useful discussion on the comparison with observations of M67. EG is supported by NWO under grant 614.000.303

References

- Alexander, D. R. & Ferguson, J. W. 1994, *ApJ*, 437, 879
- Anders, E. & Grevesse, N. 1989, *Geochim. Cosmochim. Acta*, 53, 197
- Bailyn, C. D. & Pinsonneault, M. H. 1995, *ApJ*, 439, 705
- Böhm-Vitense, E. 1958, *ZsAp*, 46, 108
- Bonatto, C., Bica, E., & Santos, Jr., J. F. C. 2005, *A&A*, 433, 917
- Carraro, G., Chiosi, C., Bressan, A., & Bertelli, G. 1994, *A&AS*, 103, 375
- Caughlan, G. R. & Fowler, W. A. 1988, *Atomic Data and Nuclear Data Tables*, 40, 283
- Caughlan, G. R., Fowler, W. A., Harris, M. J., & Zimmerman, B. A. 1985, *Atomic Data and Nuclear Data Tables*, 32, 197
- Eggleton, P. P. 1971, *MNRAS*, 151, 351
- Eggleton, P. P. 1972, *MNRAS*, 156, 361
- Endal, A. S. & Sofia, S. 1976, *ApJ*, 210, 184
- Freitag, M. & Benz, W. 2005, *MNRAS*, 358, 1133
- Girardi, L., Bertelli, G., Bressan, A., et al. 2002, *A&A*, 391, 195
- Glebbeek, E., Pols, O. R., & Hurley, J. R. 2008, submitted
- Heger, A., Langer, N., & Woosley, S. E. 2000, *ApJ*, 528, 368
- Hurley, J. R., Pols, O. R., Aarseth, S. J., & Tout, C. A. 2005, *MNRAS*, 363, 293
- Hurley, J. R., Pols, O. R., & Tout, C. A. 2000, *MNRAS*, 315, 543
- Hurley, J. R., Tout, C. A., Aarseth, S. J., & Pols, O. R. 2001, *MNRAS*, 323, 630
- Hurley, J. R., Tout, C. A., & Pols, O. R. 2002, *MNRAS*, 329, 897
- Kippenhahn, R., Ruschenplatt, G., & Thomas, H.-C. 1980, *A&A*, 91, 175
- Kippenhahn, R. & Weigert, A. 1990, *Stellar Structure and Evolution (Stellar Structure and Evolution, XVI, 468 pp. 192 figs.. Springer-Verlag Berlin Heidelberg New York. Also Astronomy and Astrophysics Library)*
- Kurucz, R. L. 1992, in *IAU Symposium, Vol. 149, The Stellar Populations of Galaxies*, ed. B. Barbuy & A. Renzini, 225–+
- Lejeune, T., Cuisinier, F., & Buser, R. 1997, *A&AS*, 125, 229
- Lombardi, Jr., J. C., Rasio, F. A., & Shapiro, S. L. 1996, *ApJ*, 468, 797
- Lombardi, Jr., J. C., Warren, J. S., Rasio, F. A., Sills, A., & Warren, A. R. 2002, *ApJ*, 568, 939
- Mathieu, R. D., Latham, D. W., & Griffin, R. F. 1990, *AJ*, 100, 1859
- Mathys, G. 1991, *A&A*, 245, 467
- Montgomery, K. A., Marschall, L. A., & Janes, K. A. 1993, *AJ*, 106, 181
- Pinsonneault, M. H., Kawaler, S. D., Sofia, S., & Demarque, P. 1989, *ApJ*, 338, 424
- Platais, I., Kozhurina-Platais, V., Mathieu, R. D., Girard, T. M., & van Alena, W. F. 2003, *AJ*, 126, 2922
- Pols, O. R., Schroder, K.-P., Hurley, J. R., Tout, C. A., & Eggleton, P. P. 1998, *MNRAS*, 298, 525
- Pols, O. R., Tout, C. A., Eggleton, P. P., & Han, Z. 1995, *MNRAS*, 274, 964
- Portegies Zwart, S. F., Makino, J., McMillan, S. L. W., & Hut, P. 1999, *A&A*, 348, 117
- Rogers, F. J. & Iglesias, C. A. 1992, *ApJS*, 79, 507
- Sanders, W. L. 1977, *A&AS*, 27, 89
- Sandquist, E. L. 2004, *MNRAS*, 347, 101
- Sandquist, E. L. 2005, *ApJ*, 635, L73
- Sills, A., Adams, T., & Davies, M. B. 2005, *MNRAS*, 358, 716
- Sills, A., Faber, J. A., Lombardi, Jr., J. C., Rasio, F. A., & Warren, A. R. 2001, *ApJ*, 548, 323
- Sills, A., Lombardi, Jr., J. C., Bailyn, C. D., et al. 1997, *ApJ*, 487, 290
- Tout, C. A., Aarseth, S. J., Pols, O. R., & Eggleton, P. P. 1997, *MNRAS*, 291, 732
- van den Berg, M., Verbunt, F., & Mathieu, R. D. 1999, *A&A*, 347, 866
- von Hippel, T. & Sarajedini, A. 1998, *AJ*, 116, 1789
- Weiss, A., Hillebrandt, W., Thomas, H.-C., & Ritter, H. 2004, *Cox and Giuli's Principles of Stellar Structure (Cox and Giuli's Principles of Stellar Structure, by A. Weiss, W. Hillebrandt, H.-C. Thomas, H. Ritter. Cambridge, UK: Princeton Publishing Associates Ltd, 2004.)*
- Yoon, S.-C., Langer, N., & Scheithauer, S. 2004, *A&A*, 425, 217
- Zahn, J.-P. 1992, *A&A*, 265, 115

Online Material

Table 4. Results for the $Z = 0.02$ collisions. The first three columns list the time of collision t (in Myr), the mass ratio q and the total initial mass M (in M_{\odot}). Column four gives the case for the collision (M, S or P, see §4.3). The total remnant mass M_{remnant} is smaller than the initial mass M because of mass loss in the collision. Column six gives the constant in the expression for the mass loss (3) for each of the individual collisions. Columns seven, eight and nine give the main sequence lifetime of the primary ($\tau_{\text{ms},1}$), secondary ($\tau_{\text{ms},2}$) and of a star of mass M_{remnant} (τ_{ms}). Column ten gives the actual remaining main sequence lifetime t_{ms} of the collision product. Columns eleven and twelve give the central abundance of hydrogen after the collision ($X_{\text{c},0}$) and at the beginning of the main sequence phase ($X_{\text{c,zms}}$). The final two columns give the change in \log_{10} luminosity L (in solar units) and \log_{10} effective temperature T_{eff} (in K) at the reddest point of the main sequence track (shortly before core hydrogen exhaustion).

t	q	M	Case	M_{remnant}	$\frac{(1+q)^2}{q}\phi$	$\tau_{\text{ms},1}$	$\tau_{\text{ms},2}$	τ_{ms}	t_{ms}	$X_{\text{c},0}$	$X_{\text{c,zms}}$	$\Delta \log_{10} L$	$\Delta \log_{10} T_{\text{eff}}$
2800	0.4	1.5	S	1.41	0.28	6247	181307	2413	2100	0.691	0.676	0.053	-0.004
2800	0.4	1.7	P	1.60	0.29	3337	134060	1726	1234	0.379	0.379	0.074	-0.008
2800	0.4	1.8	S	1.69	0.31	3444	114628	1478	951	0.547	0.574	0.095	-0.009
2800	0.4	1.9	P	1.77	0.32	2751	97623	1273	647	0.063	0.505	0.104	-0.014
2800	0.5	1.5	S	1.41	0.27	8644	124021	2519	2180	0.689	0.672	0.028	-0.002
2800	0.5	1.6	S	1.50	0.29	6382	102516	2103	1709	0.686	0.666	0.039	-0.001
2800	0.5	1.7	M	1.59	0.29	4458	85148	1746	1395	0.490	0.490	0.050	-0.006
2800	0.5	1.8	P	1.69	0.28	4206	70071	1474	1074	0.415	0.415	0.058	-0.006
2800	0.5	1.9	S	1.78	0.28	3438	57523	1261	1126	0.677	0.671	0.028	-0.002
2800	0.5	2.0	P	1.86	0.31	3001	47262	1104	534	0.124	0.128	0.065	-0.003
2800	0.6	1.5	S	1.40	0.28	11552	87227	2608	2253	0.685	0.674	0.016	-0.001
2800	0.6	1.6	S	1.49	0.31	8644	70071	2101	1848	0.683	0.662	0.032	-0.001
2800	0.6	1.7	S	1.58	0.30	6504	56129	1782	1475	0.679	0.645	0.034	-0.005
2800	0.6	1.8	P	1.68	0.28	4907	45016	1485	1152	0.513	0.513	0.041	-0.005
2800	0.6	1.9	P	1.78	0.27	3734	36312	1266	906	0.422	0.422	0.049	-0.005
2800	0.6	2.0	P	1.87	0.29	3461	29518	1099	711	0.349	0.348	0.060	-0.005
2800	0.6	2.1	P	1.94	0.32	3159	24457	984	3	0.328	0.328	0.075	-0.004
2800	0.6	2.2	P	2.04	0.30	2722	19931	859	431	0.048	0.048	0.084	-0.008
2800	0.8	1.5	S	1.40	0.26	19036	47262	2493	2352	0.676	0.669	0.016	-0.002
2800	0.8	1.6	S	1.49	0.29	14553	36598	2162	1910	0.672	0.664	0.014	-0.001
2800	0.8	1.7	S	1.57	0.31	11182	28644	1836	1577	0.662	0.649	0.016	-0.003
2800	0.8	1.8	M	1.67	0.29	8644	22659	1511	1259	0.586	0.586	0.021	-0.004
2800	0.8	1.9	P	1.75	0.31	6712	18089	1315	1051	0.550	0.550	0.029	-0.005
2800	0.8	2.0	P	1.86	0.29	5225	14553	1113	819	0.509	0.518	0.030	-0.003
2800	0.8	2.1	P	1.94	0.31	4861	11784	986	707	0.456	0.532	0.051	-0.007
2800	0.8	2.2	P	2.04	0.29	3956	9581	859	570	0.391	0.515	0.057	-0.007
2800	0.8	2.3	P	2.11	0.33	3445	7811	777	470	0.322	0.477	0.071	-0.008
2800	0.8	2.4	P	2.23	0.29	3001	6384	671	361	0.223	0.450	0.080	-0.009
2800	0.9	1.5	S	1.39	0.30	23930	36719	2643	2439	0.668	0.669	0.009	-0.001
2800	0.9	1.6	S	1.49	0.28	18301	28286	2135	1920	0.657	0.661	0.010	-0.002
2800	0.9	1.7	M	1.57	0.31	14150	22050	1818	1586	0.649	0.649	0.013	-0.002
2800	0.9	1.8	M	1.75	0.11	11029	17369	1324	1055	0.612	0.611	0.015	-0.002
2800	0.9	1.9	M	1.76	0.31	8644	13797	1312	1071	0.585	0.620	0.024	-0.005
2800	0.9	2.0	P	1.86	0.28	6801	11029	1111	859	0.554	0.539	0.026	-0.005
2800	1.0	1.5	M	1.39	0.30	29518	29518	2689	2415	0.668	0.668	0.013	-0.002
2800	1.0	1.6	M	1.49	0.28	22659	22659	2149	1924	0.652	0.659	0.008	-0.002
2800	1.0	1.8	M	1.67	0.29	13797	13797	1512	1293	0.623	0.630	0.020	-0.005
2800	1.0	1.9	M	1.75	0.31	10895	10895	1317	1093	0.605	0.613	0.028	-0.005
2800	1.0	2.0	M	1.86	0.28	8644	8646	1110	854	0.580	0.591	0.026	-0.004
2800	1.0	2.1	M	1.94	0.30	6885	6885	984	727	0.552	0.559	0.038	-0.006
2800	1.0	2.2	M	2.05	0.27	5493	5493	848	583	0.514	0.518	0.046	-0.006
2800	1.0	2.4	M	2.23	0.29	4206	4261	673	392	0.412	0.414	0.070	-0.009
3100	0.4	1.5	S	1.41	0.29	6247	181307	2443	2064	0.682	0.669	0.058	-0.004
3100	0.4	1.6	M	1.51	0.26	4537	156179	1869	1482	0.457	0.457	0.073	-0.008
3100	0.4	1.7	P	1.60	0.30	3337	134060	1728	1143	0.324	0.324	0.079	-0.008
3100	0.4	1.8	P	1.68	0.31	3444	114628	1487	864	0.204	0.204	0.102	-0.008
3100	0.5	1.5	S	1.41	0.28	8644	124021	2538	2149	0.689	0.666	0.031	-0.003
3100	0.5	1.6	S	1.50	0.27	6382	102516	2067	1674	0.659	0.645	0.041	-0.006
3100	0.5	1.7	P	1.58	0.31	4458	85148	1771	1341	0.465	0.465	0.054	-0.006
3100	0.5	1.8	P	1.69	0.28	4206	70071	1475	1017	0.365	0.365	0.064	-0.005
3100	0.5	1.9	S	1.78	0.28	3438	57523	1261	1126	0.677	0.671	0.028	-0.002
3100	0.5	2.0	P	1.86	0.31	3001	47262	1109	513	0.034	0.471	0.093	-0.012
3100	0.6	1.5	S	1.40	0.29	11552	87227	2534	2295	0.684	0.677	0.033	-0.001
3100	0.6	1.6	S	1.49	0.28	8644	70071	2057	1747	0.681	0.655	0.028	-0.004

Table 4. cont.

t	q	M	Case	M_{remnant}	$\frac{(1+q)^2}{q}\phi$	$\tau_{\text{ms},1}$	$\tau_{\text{ms},2}$	τ_{ms}	t_{ms}	$X_{c,0}$	$X_{c,zms}$	$\Delta \log_{10} L$	$\Delta \log_{10} T_{\text{eff}}$
3100	0.6	1.7	M	1.58	0.31	6504	56129	1799	1447	0.540	0.540	0.036	-0.006
3100	0.6	1.9	P	1.76	0.31	3734	36312	1301	885	0.387	0.387	0.056	-0.007
3100	0.6	2.0	P	1.86	0.30	3461	29518	1108	673	0.286	0.286	0.068	-0.004
3100	0.6	2.1	P	1.96	0.29	3159	24457	965	534	0.144	0.144	0.088	-0.011
3100	0.8	1.5	S	1.40	0.27	19036	47262	2480	2340	0.673	0.666	0.016	-0.002
3100	0.8	1.6	S	1.48	0.30	14553	36598	2116	1898	0.666	0.655	0.017	-0.001
3100	0.8	1.7	M	1.59	0.27	11182	28644	1768	1511	0.666	0.642	0.019	-0.005
3100	0.8	1.8	M	1.67	0.30	8644	22659	1523	1249	0.573	0.573	0.026	-0.005
3100	0.8	1.9	P	1.77	0.27	6712	18089	1275	982	0.531	0.531	0.030	-0.005
3100	0.8	2.0	P	1.86	0.28	5225	14553	1104	777	0.484	0.558	0.032	-0.004
3100	0.8	2.1	P	1.93	0.32	4861	11784	997	680	0.422	0.508	0.057	-0.007
3100	0.8	2.2	P	2.04	0.29	3956	9581	855	534	0.340	0.486	0.066	-0.008
3100	0.8	2.3	P	2.14	0.29	3445	7811	756	434	0.248	0.463	0.079	-0.008
3100	0.8	2.4	P	2.22	0.30	3001	6384	676	1	0.054	0.054	0.579	0.048
3100	0.9	1.7	M	1.57	0.31	14150	22050	1829	1568	0.646	0.643	0.014	-0.002
3100	0.9	1.8	M	1.67	0.29	11029	17369	1515	1265	0.599	0.628	0.022	-0.005
3100	0.9	2.0	P	1.85	0.29	6801	11029	1120	841	0.548	0.585	0.036	-0.006
3100	1.0	1.5	M	1.38	0.31	29518	29518	2588	2388	0.664	0.662	0.015	0.001
3100	1.0	1.6	M	1.49	0.28	22659	22659	2095	1893	0.649	0.654	0.011	-0.003
3100	1.0	1.7	M	1.57	0.31	18175	18175	1840	1575	0.633	0.642	0.014	-0.003
3100	1.0	1.8	M	1.67	0.29	13797	13797	1520	1282	0.615	0.624	0.024	-0.005
3100	1.0	1.9	M	1.77	0.27	10895	10895	1276	1038	0.593	0.601	0.031	-0.006
3100	1.0	2.0	M	1.85	0.29	8644	8646	1122	847	0.566	0.586	0.033	-0.006
3100	1.0	2.1	M	1.93	0.31	6885	6885	997	705	0.535	0.541	0.042	-0.007
3100	1.0	2.2	M	2.04	0.29	5493	5493	862	566	0.491	0.488	0.053	-0.007
3100	1.0	2.4	M	2.21	0.31	4206	4261	682	363	0.378	0.379	0.078	-0.011
3400	0.4	1.2	S	1.13	0.29	16991	314052	5263	4416	0.698	0.690	0.023	0.000
3400	0.4	1.3	S	1.23	0.28	12092	243954	3952	3439	0.691	0.683	0.028	-0.000
3400	0.4	1.4	S	1.32	0.27	8644	210585	3089	2568	0.690	0.676	0.042	-0.002
3400	0.4	1.5	S	1.42	0.27	6247	181307	2495	1968	0.689	0.657	0.055	-0.004
3400	0.4	1.6	P	1.50	0.30	4537	156179	2087	1486	0.411	0.411	0.070	-0.006
3400	0.4	1.7	P	1.60	0.28	3337	134060	1710	1038	0.262	0.262	0.080	-0.007
3400	0.4	1.8	P	1.69	0.29	3444	114628	1467	624	0.106	0.110	0.078	0.002
3400	0.5	1.5	S	1.40	0.29	8644	124021	2555	2128	0.681	0.661	0.034	-0.003
3400	0.5	1.6	M	1.50	0.28	6382	102516	2088	1682	0.502	0.639	0.048	-0.005
3400	0.5	1.7	P	1.59	0.30	4458	85148	1762	1268	0.430	0.430	0.058	-0.007
3400	0.5	1.8	P	1.68	0.30	4206	70071	1486	927	0.309	0.310	0.069	-0.006
3400	0.5	1.9	S	1.78	0.28	3438	57523	1262	1129	0.676	0.671	0.028	-0.002
3400	0.6	1.2	S	1.12	0.27	29518	162623	5079	4986	0.689	0.688	0.022	-0.001
3400	0.6	1.3	S	1.22	0.27	21253	133093	4005	3692	0.688	0.681	0.018	-0.001
3400	0.6	1.4	S	1.31	0.26	15571	108190	3152	2812	0.686	0.674	0.018	-0.001
3400	0.6	1.5	S	1.40	0.30	11552	87227	2539	2257	0.684	0.664	0.029	-0.002
3400	0.6	1.6	S	1.49	0.29	8644	70071	2131	1721	0.679	0.648	0.030	-0.004
3400	0.6	1.7	P	1.59	0.27	6504	56129	1746	1367	0.509	0.509	0.040	-0.006
3400	0.6	1.8	P	1.68	0.28	4907	45016	1487	1065	0.440	0.440	0.049	-0.006
3400	0.6	1.9	P	1.76	0.31	3734	36312	1301	830	0.335	0.335	0.060	-0.007
3400	0.6	2.0	P	1.86	0.30	3461	29518	1115	606	0.206	0.203	0.071	-0.004
3400	0.6	2.1	P	1.93	0.34	3159	24457	1000	12	0.037	0.037	0.095	-0.009
3400	0.8	1.2	S	1.12	0.26	47280	102516	4972	3149	0.686	0.684	0.008	0.009
3400	0.8	1.3	S	1.21	0.29	34390	79923	4135	16	0.682	0.680	0.000	0.001
3400	0.8	1.4	S	1.30	0.29	25450	61494	3244	2995	0.679	0.673	0.011	-0.001
3400	0.8	1.5	S	1.40	0.27	19036	47262	2492	2323	0.673	0.661	0.017	-0.002
3400	0.8	1.6	S	1.48	0.30	14553	36598	2126	1886	0.667	0.651	0.018	-0.002
3400	0.8	1.7	M	1.58	0.28	11182	28644	1780	1494	0.596	0.596	0.022	-0.005
3400	0.8	1.8	P	1.68	0.28	8644	22659	1499	1192	0.553	0.553	0.028	-0.005
3400	0.8	1.9	P	1.76	0.31	6712	18089	1311	968	0.513	0.510	0.031	-0.005
3400	0.8	2.0	P	1.85	0.29	5225	14553	1120	782	0.455	0.559	0.046	-0.007
3400	0.8	2.1	P	1.95	0.29	4861	11784	970	628	0.378	0.493	0.060	-0.009
3400	0.8	2.2	P	2.03	0.32	3956	9581	877	503	0.297	0.452	0.075	-0.009
3400	0.8	2.3	P	2.13	0.29	3445	7811	759	385	0.185	0.391	0.085	-0.010
3400	0.8	2.4	P	2.18	0.37	3001	6384	709	287	0.201	0.201	0.109	-0.015

Table 4. cont.

t	q	M	Case	M_{remnant}	$\frac{(1+q)^2}{q}\phi$	$\tau_{\text{ms},1}$	$\tau_{\text{ms},2}$	τ_{ms}	t_{ms}	$X_{\text{c},0}$	$X_{\text{c},\text{zms}}$	$\Delta \log_{10} L$	$\Delta \log_{10} T_{\text{eff}}$
3400	0.9	1.7	M	1.59	0.27	14150	22050	1764	1531	0.609	0.621	0.022	-0.004
3400	0.9	1.8	M	1.67	0.30	11029	17369	1526	1245	0.586	0.584	0.023	-0.006
3400	0.9	1.9	P	1.77	0.28	8644	13797	1280	1002	0.559	0.597	0.032	-0.006
3400	0.9	2.0	P	1.86	0.28	6801	11029	1110	801	0.510	0.569	0.037	-0.007
3400	1.0	1.2	M	1.12	0.28	70143	70071	5094	4783	0.681	0.682	0.001	-0.000
3400	1.0	1.3	M	1.20	0.31	52156	52156	4217	3971	0.677	0.678	0.006	-0.000
3400	1.0	1.4	M	1.30	0.28	38969	38969	3243	2928	0.668	0.670	0.007	0.001
3400	1.0	1.5	M	1.38	0.31	29518	29518	2691	2384	0.659	0.659	0.013	-0.001
3400	1.0	1.6	M	1.48	0.29	22659	22659	2166	1894	0.646	0.649	0.012	-0.002
3400	1.0	1.7	M	1.59	0.27	18175	18175	1753	1510	0.624	0.635	0.019	-0.005
3400	1.0	1.8	M	1.67	0.30	13797	13797	1528	1227	0.620	0.605	0.013	-0.006
3400	1.0	2.0	M	1.85	0.30	8644	8646	1132	818	0.552	0.574	0.033	-0.006
3400	1.0	2.1	M	1.95	0.28	6885	6885	970	662	0.512	0.519	0.048	-0.007
3400	1.0	2.2	M	2.03	0.32	5493	5493	876	541	0.467	0.470	0.059	-0.008
3400	1.0	2.4	M	2.22	0.30	4206	4261	676	328	0.325	0.326	0.085	-0.013
3700	0.4	1.2	S	1.14	0.25	16991	314052	4881	4436	0.698	0.687	0.039	-0.000
3700	0.4	1.3	S	1.22	0.29	12092	243954	3962	3405	0.691	0.682	0.034	-0.000
3700	0.4	1.4	S	1.32	0.29	8644	210585	3113	2540	0.690	0.674	0.046	-0.002
3700	0.4	1.5	S	1.41	0.28	6247	181307	2526	1932	0.667	0.648	0.061	-0.004
3700	0.4	1.8	P	1.68	0.34	3444	114628	1501	667	0.032	0.467	0.114	-0.017
3700	0.5	1.5	S	1.41	0.26	8644	124021	2507	2054	0.678	0.656	0.038	-0.004
3700	0.5	1.6	P	1.49	0.30	6382	102516	2111	1610	0.479	0.479	0.050	-0.006
3700	0.5	1.7	P	1.59	0.29	4458	85148	1747	1196	0.391	0.391	0.063	-0.007
3700	0.5	1.8	P	1.68	0.31	4206	70071	1494	850	0.251	0.251	0.070	-0.006
3700	0.5	1.9	S	1.78	0.28	3438	57523	1263	1120	0.672	0.669	0.029	-0.002
3700	0.6	1.2	S	1.12	0.27	29518	162623	4958	2885	0.689	0.686	0.008	0.001
3700	0.6	1.3	S	1.22	0.27	21253	133093	4010	3642	0.688	0.679	0.018	-0.000
3700	0.6	1.4	S	1.31	0.27	15571	108190	3181	2796	0.686	0.672	0.018	-0.001
3700	0.6	1.5	S	1.41	0.27	11552	87227	2479	2176	0.680	0.660	0.033	-0.002
3700	0.6	1.6	M	1.49	0.30	8644	70071	2094	1699	0.677	0.645	0.035	-0.004
3700	0.6	1.7	P	1.59	0.28	6504	56129	1765	1335	0.501	0.501	0.042	-0.006
3700	0.6	1.8	P	1.68	0.28	4907	45016	1480	1010	0.403	0.403	0.052	-0.007
3700	0.6	1.9	P	1.77	0.29	3734	36312	1275	753	0.283	0.283	0.060	-0.006
3700	0.6	2.0	P	1.85	0.33	3461	29518	1133	556	0.120	0.134	0.094	-0.012
3700	0.8	1.2	S	1.12	0.26	47280	102516	4972	3149	0.686	0.684	0.001	0.000
3700	0.8	1.3	S	1.21	0.29	34390	79923	4160	3844	0.682	0.678	0.003	-0.000
3700	0.8	1.4	S	1.30	0.29	25450	61494	3261	2972	0.676	0.669	0.012	-0.001
3700	0.8	1.5	S	1.40	0.28	19036	47262	2624	2303	0.658	0.657	0.009	-0.002
3700	0.8	1.6	M	1.48	0.31	14553	36598	2137	1862	0.659	0.644	0.018	-0.002
3700	0.8	1.7	M	1.58	0.29	11182	28644	1790	1466	0.589	0.589	0.022	-0.005
3700	0.8	1.8	P	1.67	0.29	8644	22659	1512	1172	0.541	0.541	0.030	-0.006
3700	0.8	1.9	P	1.75	0.32	6712	18089	1325	931	0.492	0.526	0.032	-0.004
3700	0.8	2.0	P	1.84	0.32	5225	14553	1141	761	0.428	0.545	0.050	-0.008
3700	0.8	2.1	P	1.94	0.30	4861	11784	985	619	0.345	0.463	0.071	-0.008
3700	0.8	2.2	P	2.03	0.31	3956	9581	869	481	0.233	0.425	0.081	-0.010
3700	0.8	2.3	P	2.12	0.32	3445	7811	772	1	0.050	0.050	0.153	0.060
3700	0.9	1.5	S	1.40	0.26	23930	36719	2528	2296	0.654	0.657	0.013	-0.003
3700	0.9	1.6	M	1.48	0.29	18301	28286	2160	1871	0.650	0.647	0.014	-0.003
3700	0.9	1.7	M	1.57	0.30	14150	22050	1808	1497	0.599	0.599	0.017	-0.004
3700	0.9	1.8	M	1.67	0.28	11029	17369	1503	1204	0.572	0.572	0.026	-0.006
3700	0.9	1.9	P	1.75	0.31	8644	13797	1319	958	0.541	0.582	0.026	-0.004
3700	0.9	2.0	P	1.85	0.29	6801	11029	1121	777	0.492	0.558	0.040	-0.006
3700	1.0	1.2	M	1.12	0.28	70143	70071	5094	4783	0.681	0.682	0.001	-0.000
3700	1.0	1.3	M	1.20	0.31	52156	52156	4228	4030	0.675	0.675	0.001	0.000
3700	1.0	1.4	M	1.30	0.28	38969	38969	3236	2988	0.665	0.667	0.009	-0.001
3700	1.0	1.5	M	1.40	0.26	29518	29518	2598	2268	0.650	0.651	0.010	-0.000
3700	1.0	1.6	M	1.48	0.29	22659	22659	2178	1878	0.636	0.645	0.013	-0.002
3700	1.0	1.7	M	1.58	0.28	18175	18175	1780	1490	0.618	0.625	0.018	-0.005
3700	1.0	1.8	M	1.66	0.31	13797	13797	1542	1196	0.597	0.596	0.013	-0.005
3700	1.0	1.9	M	1.76	0.29	10895	10895	1296	997	0.572	0.582	0.036	-0.007
3700	1.0	2.0	M	1.84	0.32	8644	8646	1136	783	0.537	0.554	0.035	-0.005

Table 4. cont.

t	q	M	Case	M_{remnant}	$\frac{(1+q)^2}{q}\phi$	$\tau_{\text{ms},1}$	$\tau_{\text{ms},2}$	τ_{ms}	t_{ms}	$X_{\text{c},0}$	$X_{\text{c,zms}}$	$\Delta \log_{10} L$	$\Delta \log_{10} T_{\text{eff}}$
3700	1.0	2.1	M	1.94	0.30	6885	6885	983	641	0.493	0.492	0.053	-0.008
3700	1.0	2.2	M	2.04	0.29	5493	5493	861	411	0.436	0.436	0.001	0.000
3700	1.0	2.4	M	2.20	0.34	4206	4261	695	305	0.281	0.281	0.098	-0.015
4200	0.4	1.2	S	1.14	0.26	16991	314052	5119	4442	0.698	0.684	0.031	0.000
4200	0.4	1.3	S	1.23	0.26	12092	243954	3890	3272	0.689	0.676	0.037	-0.001
4200	0.4	1.4	S	1.33	0.26	8644	210585	3052	2379	0.688	0.666	0.058	-0.000
4200	0.6	1.2	S	1.12	0.29	29518	162623	5056	4728	0.688	0.684	0.028	0.000
4200	0.6	1.3	S	1.22	0.28	21253	133093	4050	3623	0.685	0.676	0.018	-0.001
4200	0.6	1.4	S	1.31	0.28	15571	108190	3191	2755	0.683	0.666	0.022	-0.002
4200	0.8	1.2	S	1.12	0.27	47280	102516	5003	4701	0.683	0.681	0.014	0.000
4200	0.8	1.3	S	1.20	0.30	34390	79923	4157	3820	0.679	0.675	0.005	-0.000
4200	0.8	1.4	S	1.30	0.30	25450	61494	3273	2948	0.673	0.665	0.013	-0.001
4200	1.0	1.2	M	1.12	0.28	70143	70071	5117	4757	0.678	0.679	0.001	0.000
4200	1.0	1.3	M	1.22	0.26	52156	52156	4049	270	0.670	0.671	0.004	0.000
4200	1.0	1.4	M	1.30	0.29	38969	38969	3256	2953	0.659	0.661	0.010	-0.001
4200	1.0	2.2	M	2.04	0.30	5493	5493	864	454	0.386	0.386	0.083	-0.011
4700	0.4	1.2	S	1.13	0.27	16991	314052	4934	4420	0.698	0.682	0.062	-0.000
4700	0.4	1.3	S	1.23	0.28	12092	243954	3930	3213	0.687	0.671	0.042	-0.001
4700	0.4	1.4	S	1.32	0.28	8644	210585	3103	2310	0.686	0.669	0.058	-0.003
4700	0.6	1.2	S	1.13	0.25	29518	162623	5176	4571	0.684	0.681	0.006	0.001
4700	0.6	1.3	S	1.21	0.28	21253	133093	4072	12	0.685	0.673	0.007	0.000
4700	0.6	1.4	S	1.31	0.29	15571	108190	3215	2720	0.680	0.660	0.025	-0.002
4700	0.8	1.2	S	1.12	0.27	47280	102516	5023	4810	0.680	0.678	0.021	0.000
4700	0.8	1.3	S	1.20	0.30	34390	79923	486	14	0.676	0.671	0.000	0.000
4700	0.8	1.4	S	1.29	0.31	25450	61494	3299	3009	0.670	0.659	0.035	-0.006
4700	1.0	1.2	M	1.11	0.28	70143	70071	5140	4725	0.675	0.676	0.000	-0.000
4700	1.0	1.3	M	1.21	0.27	52156	52156	4059	3848	0.667	0.667	0.006	-0.000
4700	1.0	1.4	M	1.30	0.30	38969	38969	3275	2922	0.652	0.655	0.011	-0.001
4700	1.0	2.2	M	2.03	0.32	5493	5493	877	431	0.329	0.329	0.100	-0.015
5200	0.4	1.2	S	1.13	0.29	16991	314052	5253	4375	0.698	0.680	0.044	0.001
5200	0.4	1.3	S	1.22	0.29	12092	243954	3955	3166	0.687	0.669	0.050	-0.001
5200	0.4	1.4	M	1.33	0.26	8644	210585	3061	2251	0.447	0.421	0.067	-0.004
5200	0.6	1.2	S	1.13	0.25	29518	162623	5250	4687	0.684	0.679	0.020	0.000
5200	0.6	1.3	S	1.22	0.26	21253	133093	3970	3471	0.682	0.668	0.020	-0.001
5200	0.6	1.4	S	1.31	0.26	15571	108190	3153	2628	0.679	0.653	0.029	-0.002
5200	0.8	1.2	S	1.12	0.27	47280	102516	5048	2917	0.680	0.676	0.000	0.000
5200	0.8	1.3	S	1.22	0.26	34390	79923	75	3614	0.672	0.666	0.277	-0.006
5200	0.8	1.4	S	1.29	0.31	25450	61494	3311	2888	0.667	0.653	0.016	-0.002
5200	1.0	1.2	M	1.11	0.29	70143	70071	5162	4703	0.672	0.673	0.001	-0.000
5200	1.0	1.3	M	1.21	0.27	52156	52156	4073	3689	0.661	0.662	0.009	-0.001
5200	1.0	1.4	M	1.30	0.30	38969	38969	3286	2910	0.649	0.652	0.012	-0.001
5200	1.0	2.2	M	2.02	0.32	5493	5493	880	379	0.263	0.263	0.125	-0.018
5700	0.4	1.2	S	1.13	0.30	16991	314052	4884	3914	0.698	0.677	0.009	-0.002
5700	0.4	1.3	S	1.23	0.26	12092	243954	3897	3022	0.684	0.661	0.053	-0.001
5700	0.6	1.2	S	1.13	0.26	29518	162623	4626	4641	0.681	0.675	0.081	-0.001
5700	0.6	1.3	S	1.22	0.26	21253	133093	3551	3463	0.679	0.664	0.125	0.005
5700	0.6	1.4	S	1.31	0.27	15571	108190	3174	2592	0.676	0.647	0.032	-0.003
5700	0.8	1.2	S	1.12	0.28	47280	102516	5068	4926	0.677	0.673	0.041	-0.001
5700	0.8	1.3	S	1.22	0.26	34390	79923	4040	13	0.669	0.662	0.004	0.000
5700	0.8	1.4	S	1.31	0.27	25450	61494	3197	2742	0.662	0.648	0.014	-0.002
5700	1.0	1.2	M	1.11	0.29	70143	70071	5183	4664	0.669	0.671	0.000	-0.000
5700	1.0	1.3	M	1.21	0.27	52156	52156	4127	3669	0.658	0.659	0.004	-0.000
5700	1.0	1.4	M	1.29	0.31	38969	38969	3304	2876	0.643	0.646	0.014	-0.001

Table 3. As Table 4 for the $Z = 0.001$ models.

t	q	M	Case	M_{remnant}	$\frac{(1+q)^{\gamma}}{q}\phi$	$\tau_{\text{ms},1}$	$\tau_{\text{ms},2}$	τ_{ms}	t_{ms}	$X_{\text{c},0}$	$X_{\text{c},\text{zms}}$	$\Delta \log_{10} L$	$\Delta \log_{10} T_{\text{eff}}$
8000	0.4	0.8	S	0.76	0.25	43810	695587	14678	13000	0.753	0.751	0.018	0.001
8000	0.4	0.9	S	0.85	0.25	27922	544208	9331	7683	0.752	0.719	0.032	0.002
8000	0.4	1.0	S	0.95	0.25	18612	418946	6214	4645	0.752	0.701	0.062	0.006
8000	0.4	1.1	P	1.04	0.27	12867	313659	4353	2459	0.408	0.403	0.066	0.010
8000	0.4	1.2	P	1.13	0.29	9181	221923	3150	3	0.210	0.210	0.000	0.089
8000	0.6	0.8	S	0.76	0.24	72663	364938	14963	13905	0.752	0.752	0.015	0.001
8000	0.6	0.9	S	0.85	0.24	46528	236659	9496	8484	0.751	0.746	0.016	0.001
8000	0.6	1.0	S	0.93	0.28	31103	178559	6579	5470	0.730	0.722	0.019	0.001
8000	0.6	1.1	M	1.03	0.27	21571	138218	4513	2827	0.573	0.541	0.030	0.001
8000	0.6	1.2	P	1.12	0.28	15409	105374	3241	1986	0.485	0.485	0.027	0.004
8000	0.6	1.3	P	1.22	0.28	11298	79734	2354	935	0.348	0.350	0.028	0.006
8000	0.8	0.8	S	0.75	0.25	109778	202645	15353	14290	0.735	0.733	0.004	0.000
8000	0.8	0.9	S	0.85	0.24	72663	150804	9633	8725	0.727	0.727	0.004	0.000
8000	0.8	1.0	S	0.94	0.25	48790	109778	6487	5614	0.720	0.713	0.006	0.000
8000	0.8	1.2	P	1.12	0.26	24284	57012	3215	2305	0.592	0.592	0.011	0.001
8000	0.8	1.3	P	1.21	0.30	17831	41997	2441	1493	0.526	0.527	0.025	0.002
8000	1.0	0.8	M	0.75	0.26	150804	150804	15550	14471	0.729	0.729	0.003	0.000
8000	1.0	0.9	M	0.84	0.27	105374	105374	9911	9016	0.720	0.720	0.003	0.000
8000	1.0	1.0	M	0.93	0.27	72663	72663	6603	5773	0.705	0.705	0.003	0.000
8000	1.0	1.1	M	1.03	0.26	50701	50701	4509	3695	0.682	0.683	0.008	0.001
8000	1.0	1.2	M	1.12	0.26	36358	36358	3218	2388	0.649	0.651	0.007	0.001
8000	1.0	1.3	M	1.21	0.29	26764	26764	2425	1596	0.612	0.612	0.024	0.001
9500	0.4	0.8	S	0.76	0.26	43810	695587	14847	12884	0.752	0.752	0.023	0.002
9500	0.4	0.9	S	0.85	0.27	27922	544208	9479	7438	0.751	0.709	0.037	0.002
9500	0.4	1.0	S	0.94	0.28	18612	418946	6367	4278	0.751	0.680	0.052	0.006
9500	0.4	1.1	P	1.04	0.28	12867	313659	4403	2057	0.313	0.313	0.069	0.011
9500	0.4	1.2	P	1.13	0.29	9181	221923	3151	235	0.047	0.069	0.079	0.017
9500	0.6	0.8	S	0.75	0.24	72663	364938	15051	13767	0.751	0.750	0.015	0.001
9500	0.6	0.9	S	0.85	0.25	46528	236659	1009	8353	0.751	0.729	0.500	0.025
9500	0.6	1.0	S	0.94	0.25	31103	178559	6412	5105	0.723	0.705	0.022	0.002
9500	0.6	1.1	P	1.03	0.26	21571	138218	4469	3073	0.528	0.528	0.028	0.003
9500	0.6	1.2	P	1.12	0.28	15409	105374	3247	1695	0.414	0.415	0.031	0.004
9500	0.6	1.3	P	1.21	0.30	11298	79734	2420	621	0.235	0.235	0.032	0.007
9500	0.8	0.8	S	0.75	0.26	109778	202645	15447	14171	0.729	0.728	0.006	0.000
9500	0.8	0.9	S	0.84	0.25	72663	150804	9702	8612	0.722	0.720	0.005	0.000
9500	0.8	1.1	M	1.02	0.28	33896	78905	4632	3545	0.620	0.631	0.010	0.002
9500	0.8	1.2	P	1.12	0.28	24284	57012	3279	2173	0.557	0.557	0.014	0.002
9500	0.8	1.3	P	1.20	0.30	17831	41997	2336	1285	0.470	0.470	0.050	0.003
9500	1.0	0.8	M	0.75	0.27	150804	150804	15638	14353	0.724	0.724	0.002	0.000
9500	1.0	0.9	M	0.84	0.27	105374	105374	9974	8906	0.713	0.713	0.003	0.000
9500	1.0	1.0	M	0.93	0.28	72663	72663	6663	5653	0.695	0.695	0.004	0.000
9500	1.0	1.1	M	1.03	0.27	50701	50701	4584	3588	0.667	0.667	0.007	0.001
9500	1.0	1.2	M	1.12	0.27	36358	36358	3271	2264	0.627	0.631	0.010	0.001
9500	1.0	1.3	M	1.21	0.26	26764	26764	2368	1410	0.574	0.579	0.032	0.001
11000	0.4	0.8	S	0.76	0.28	43810	695587	14999	12605	0.751	0.746	0.028	0.002
11000	0.4	0.9	S	0.85	0.25	27922	544208	9333	7069	0.751	0.710	0.054	0.005
11000	0.4	1.0	P	0.94	0.28	18612	418946	6329	3858	0.420	0.420	0.059	0.006
11000	0.4	1.1	P	1.03	0.30	12867	313659	4484	1377	0.211	0.211	0.036	0.011
11000	0.6	0.8	S	0.75	0.25	72663	364938	15139	13640	0.750	0.749	0.015	0.001
11000	0.6	0.9	S	0.85	0.26	46528	236659	9674	8250	0.750	0.737	0.023	0.002
11000	0.6	1.0	M	0.94	0.27	31103	178559	6499	4849	0.696	0.536	0.010	0.002
11000	0.6	1.1	P	1.03	0.25	21571	138218	4434	2770	0.480	0.480	0.030	0.003
11000	0.6	1.2	P	1.12	0.29	15409	105374	3264	1322	0.336	0.336	0.026	0.005
11000	0.6	1.3	P	1.21	0.29	11298	79734	2383	306	0.104	0.134	0.071	0.009
11000	0.8	0.8	S	0.75	0.26	109778	202645	15514	14031	0.724	0.724	0.005	0.000
11000	0.8	0.9	S	0.84	0.27	72663	150804	9928	8636	0.717	0.713	0.005	0.000
11000	0.8	1.1	P	1.02	0.30	33896	78905	4696	3407	0.596	0.596	0.012	0.002
11000	0.8	1.2	P	1.12	0.27	24284	57012	3257	1940	0.516	0.516	0.015	0.002
11000	0.8	1.3	P	1.21	0.28	17831	41997	2401	1026	0.407	0.407	0.019	0.002
11000	1.0	0.8	M	0.75	0.27	150804	150804	15694	14943	0.720	0.720	0.000	0.000

Table 3. cont.

t	q	M	Case	M_{remnant}	$\frac{(1+q)^2}{q}\phi$	$\tau_{\text{ms},1}$	$\tau_{\text{ms},2}$	τ_{ms}	t_{ms}	$X_{\text{c},0}$	$X_{\text{c},\text{zms}}$	$\Delta \log_{10} L$	$\Delta \log_{10} T_{\text{eff}}$
11000	1.0	0.9	M	0.84	0.28	105374	105374	10036	751	0.706	0.706	0.000	0.000
11000	1.0	1.0	M	0.93	0.28	72663	72663	6723	5559	0.685	0.685	0.003	0.000
11000	1.0	1.1	M	1.02	0.28	50701	50701	4639	3473	0.653	0.653	0.007	0.001
11000	1.0	1.2	M	1.11	0.29	36358	36358	3332	2125	0.606	0.606	0.011	0.001
11000	1.0	1.3	M	1.21	0.29	26764	26764	2321	1175	0.541	0.545	0.025	0.001
12500	0.4	0.9	S	0.85	0.27	27922	544208	9492	6505	0.750	0.690	0.014	0.004
12500	0.4	1.0	P	0.94	0.27	18612	418946	6304	3365	0.355	0.355	0.067	0.007
12500	0.4	1.1	P	1.03	0.29	12867	313659	4440	492	0.095	0.096	0.047	0.016
12500	0.6	0.8	S	0.75	0.26	72663	364938	15230	13508	0.750	0.747	0.017	0.001
12500	0.6	0.9	S	0.85	0.24	46528	236659	9475	7857	0.748	0.718	0.025	0.002
12500	0.6	1.0	M	0.94	0.25	31103	178559	6399	4582	0.546	0.546	0.027	0.002
12500	0.6	1.1	P	1.03	0.28	21571	138218	4537	2526	0.433	0.433	0.029	0.004
12500	0.6	1.2	P	1.12	0.30	15409	105374	3301	918	0.249	0.249	0.022	0.007
12500	0.8	0.8	S	0.75	0.27	109778	202645	15605	13908	0.720	0.719	0.007	0.000
12500	0.8	0.9	S	0.84	0.28	72663	150804	10004	8516	0.712	0.706	0.007	0.000
12500	0.8	1.0	M	0.94	0.26	48790	109778	6515	5108	0.630	0.633	0.008	0.001
12500	0.8	1.1	P	1.03	0.27	33896	78905	4552	3115	0.567	0.567	0.013	0.002
12500	0.8	1.2	P	1.11	0.29	24284	57012	3326	1796	0.476	0.476	0.016	0.002
12500	0.8	1.3	P	1.21	0.27	17831	41997	2366	817	0.338	0.338	0.027	0.002
12500	1.0	0.8	M	0.75	0.23	150804	150804	15091	13462	0.712	0.711	0.003	0.000
12500	1.0	0.9	M	0.84	0.28	105374	105374	10100	8680	0.699	0.699	0.004	0.000
12500	1.0	1.0	M	0.94	0.25	72663	72663	6464	5187	0.672	0.672	0.003	0.000
12500	1.0	1.1	M	1.02	0.29	50701	50701	4705	3866	0.639	0.639	0.003	0.001
12500	1.0	1.2	M	1.12	0.26	36358	36358	3235	1911	0.576	0.580	0.012	0.001
12500	1.0	1.3	M	1.21	0.27	26764	26764	2376	1126	0.502	0.507	0.049	0.002